OPEN ACCESS

UNIVERSITY OF THE
WEST of SCOTLAND
UWS

UWS Academic Portal

Experimental study of the lifetime and phase transition in neutron-rich 98,100,102Zr

Ansari, S.; Régis, J.-M.; Jolie, J.; Saed-Samii, N.; Warr, N.; Korten, W.; Zieliska, M.; Salsac, M.-D.; Blanc, A.; Jentschel, M.; Köster, U.; Mutti, P.; Soldner, T.; Simpson, G. S.; Drouet, F.; Vancraeyenest, A.; De France, G.; Clément, E.; Stezowski, O.; Ur, C. A.; Urban, W.; Regan, P. H.; Podolyák, Zs.; Larijani, C.; Townsley, C.; Carroll, R.; Wilson, E.; Mach, H.; Fraile, L.M.; Paziy, V.; Olaizola, B.; Vedia, V.; Bruce, A. M.; Roberts, O. J.; Smith, J. F.; Scheck, M.; Kröll, T.; Hartig, A.-L.; Ignatov, A.; Ilieva, S.; Lalkovski, S.; Mrginean, N.; Otsuka, T.; Shimizu, N.; Togashi, T.; Tsunoda, Y.

Document Version
Peer reviewed version

Link to publication on the UWS Academic Portal

Study of lifetime and phase transition in neutron-rich ^{98,100,102}Zr

S. Ansari,[1,2] J.-M. Régis,[1] J. Jolie,[1] N. Saed-Samii,[1] N. Warr,[1] W. Korten,[2] M. Zielińska,[2] M.-D. Salsac,[2]

A. Blanc,[3] M. Jentschel,[3] U. Köster,[3] P. Mutti,[3] T. Soldner,[3] G.S. Simpson,[4] F. Drouet,[4] A. Vancraeyenest,[4]

G. de France,[5] E. Clément,[5] O. Stezowski,[6] C.A. Ur,[7] W. Urban,[8] P.H. Regan,[9,10] Zs. Podolyák,[9] C. Larijani,[9,10]

C. Townsley,[9] R. Carroll,[9] E. Wilson,[9] H. Mach,[11,*] L.M. Fraile,[12] V. Paziy,[12] B. Olaizola,[12,13] V. Vedia,[12]

A.M. Bruce,[14] O.J. Roberts,[14] J.F. Smith,[15] M. Scheck,[15] T. Kröll,[16] A.-L. Hartig,[16] A. Ignatov,[16] S. Ilieva,[16]

S. Lalkovski,[17] N. Mărginean,[18] T. Otsuka,[19,20,21,22,23] N. Shimizu,[20] T. Togashi,[20] and Y. Tsunoda[20]

[1]*Institut für Kernphysik der Universität zu Köln, Zülpicher Str. 77, 50937 Köln, Germany*
[2]*Irfu, CEA, Université Paris-Saclay, F-91191 Gif-sur-Yvette, France*[†]
[3]*Institut Laue-Langevin, 71 avenue des Martyrs, 38042 Grenoble Cedex, France*
[4]*LPSC, 53 avenue des Martyrs, 38026 Grenoble Cedex, France*
[5]*Grand Accélérateur National d'Ions Lourds (GANIL),*
CEA/CRF-CNRS/IN2P3, 14076 Caen Cedex 05, France
[6]*IPN de Lyon, 4, Rue Enrico Fermi, 69622 Villeurbanne Cedex, France*
[7]*INFN, via Marzolo 8, 35131 Padova, Italy*
[8]*Faculty of Physics, University of Warsaw, ul. Pasteura 5, 02-093, Warsaw, Poland*
[9]*Department of Physics, University of Surrey, Guildford GU2 7XH, United Kingdom*
[10]*National Physical Laboratory, Teddington, Middlesex, TW11 0LW, United Kingdom*
[11]*National Centre for Nuclear Research, Andrzeja Sołtana 7, 05-400 Otwock-Świerk, Poland*
[12]*Grupo de Fisica Nuclear, FAMN, Universidad Complutense, 28040 Madrid, Spain*
[13]*TRIUMF, 4004 Wesbrook Mall, Vancouver, BC, V6T 2A3, Canada*
[14]*School of Computing, Engineering and Mathematics,*
University of Brighton, Brighton, BN2 4GJ, United Kingdom
[15]*School of Engineering and Computing, University of the West of Scotland, High Street, Paisley, PA1 2BE, United Kingdom*
[16]*Institut für Kernphysik, TU Darmstadt, Schlossgartenstr. 7, 64289 Darmstadt, Germany*
[17]*Faculty of Physics, University of Sofia, 1164 Sofia, Bulgaria*
[18]*Horia Hulubei NIPNE, 77125 Bucharest, Romania*
[19]*RIKEN Nishina Center, 2-1 Hirosawa, Wako, Saitama 351-0198, Japan*
[20]*Center for Nuclear Study, University of Tokyo, Hongo, Bunkyo-ku Tokyo 113-0033, Japan*
[21]*Department of Physics, University of Tokyo, Hongo, Bunkyo-ku Tokyo 113-0033, Japan*
[22]*NSCL, Michigan State University, East Lansing, Michigan 48824, USA*
[23]*Instituut voor Kern- en Stralingsfysica, KU Leuven, B-3001 Leuven, Belgium*
(Dated: November 15, 2017)

Rapid shape changes are observed for neutron-rich nuclei with A around 100. In particular, a sudden onset of ground-state deformation is observed in the Zr and Sr isotopic chains at N=60: low-lying states in N≤58 nuclei are nearly spherical, while those with N≥60 have a rotational character. Nuclear lifetimes as short as a few ps can be measured using fast-timing techniques with LaBr$_3$(Ce)-scintillators, yielding a key ingredient in the systematic study of the shape evolution in this region. We used neutron-induced fission of ^{241}Pu and ^{235}U to study lifetimes of excited states in fission fragments in the A~100 region with the EXILL-FATIMA array located at the PF1B cold neutron beam line at the Institut Laue-Langevin. In particular, we applied the generalized centroid difference method to deduce lifetimes of low-lying states for the nuclei ^{98}Zr (N=58), ^{100}Zr and ^{102}Zr (N≥60). The results are discussed in the context of the presumed phase transition in the Zr chain by comparing the experimental transition strengths with the theoretical calculations using the Interacting Boson Model and the Monte Carlo Shell Model.

I. INTRODUCTION

The last few decades have seen a focus on the shape-phase transition in nuclei around A=100. The appearance of strong quadrupole deformation beyond N=60 in the A~100 mass region was discovered in the 1960's by S.A.E. Johansson [1] in a study of γ rays emitted by fission fragments. Soon after, Cheifetz *et al*. [2] observed regular rotational bands in neutron-rich Zr, Mo, Ru and Pd isotopes populated in spontaneous fission of ^{252}Cf. In particular, the lifetimes of the 2^+_1 states in ^{100,102}Zr obtained in that study [2] confirmed their highly-deformed character. These experimental discoveries triggered an important theoretical effort to explain the origin of quadrupole deformation in A~100 nuclei; early calculations are described for example in Refs. [3, 4].

The simplest estimate of nuclear deformation can be obtained from the energy of the 2^+_1 state in even-even nuclei. For Sr (Z=38) and Zr (Z=40) isotopes it is observed to decrease dramatically at N=60, while the evolution is much more gradual in Mo nuclei (Z=42) (see Fig. 1). A gradual decrease of

---

the 2^+_1 energy is also observed for ^{92,94,96}Kr nuclei (Z=36). This is consistent with the results of mass measurements for ^{96,97}Kr [5] that show a smooth evolution towards the dripline in contrast to the sharp changes observed for heavier N=60 nuclei. However, a significant drop in energy was observed for the 2^+_1 state in ^{98}Kr [6]. This energy further stabilized at ^{100}Kr [6], which suggests that a shape transition may appear in the Kr isotopic chain at N=62 instead of N=60. Judging by level energies alone, the Z-boundaries of the region of the shape transition at N=60 seem to be clearly defined.
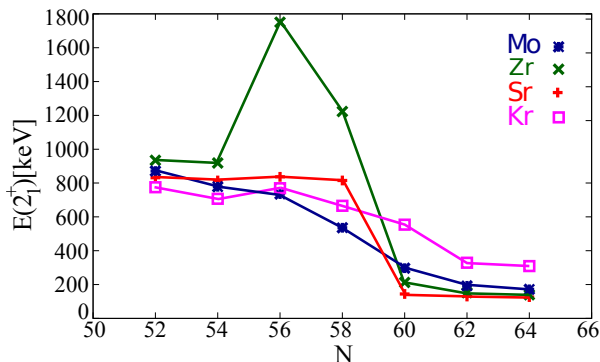

FIG. 1. Evolution of the 2^+_1 excitation energy as a function of neutron number in the A ∼ 100 region. The transition energies are taken from National Nuclear Data Center [7] and the recent results for ^{98,100}Kr are adopted from Ref. [6]

The $R_{4/2} = E(4^+_1)/E(2^+_1)$ ratios for N≥60 Sr, Zr, Mo and Ru nuclei have a value around 3 [2], which is expected for a rigid rotor and is consistent with a static character of the deformation in this mass region. Again, a very different behavior has recently been observed in ^{96}Kr, with the $R_{4/2}$ value dropping abruptly to 2.1, suggesting a dynamical character of the deformation [8].

A similar picture is emerging from measurements of transition probabilities. A Coulomb excitation study of ^{96}Kr [9] yielded a B(E2; $2^+_1 \longrightarrow 0^+_1$) value much lower than those for ^{98}Sr and ^{100}Zr, and only slightly higher than that for ^{94}Kr [9]. In contrast, regular rotational ground-state bands were observed in ^{97,99}Rb [10], and the obtained transition probabilities show that the deformation of these nuclei is essentially the same as that observed inside the well-deformed region, thus establishing ^{97}Rb as its cornerstone. Recent lifetime measurements for ^{99,101}Y and ^{101,103,105}Nb [11] confirmed that these nuclei are as deformed as the neighboring even-even isotopes with N≥60.

Sudden shape changes may be interpreted as a result of an inversion of two distinct configurations associated with different nuclear shapes. Indeed, the shape transition at N=60 is accompanied by the appearance of low-lying 0^+_2 states indicating possible shape coexistence [12] and, similar to the 2^+_1 state, an abrupt drop of the 0^+_2 energy is observed at N=60. The recent Coulomb excitation study of ^{96,98}Sr [13, 14] provided firm evidence for configuration inversion in these nuclei, demonstrating important similarities in terms of transition probabilities

and spectroscopic quadrupole moments between the ground-state band in ^{96}Sr and the structure built on the 0^+_2 state in ^{98}Sr. These conclusions are consistent with the results of a new lifetime measurement in the Sr isotopic chain [15]. The interpretation of E2 matrix elements obtained in the Coulomb excitation measurement [13, 14] using the two-state mixing model points to very low mixing between prolate and spherical configurations in the wave functions of the 0^+_1 states in ^{98}Sr, in spite of their proximity in energy. The same conclusion can be drawn from the measured E0 transition strength between the 0^+_2 and the 0^+_1 states in ^{98}Sr [16, 17] and also from E0 and E2 transition strengths in ^{100}Zr [18–20]. The weak mixing of the coexisting structures in ^{98}Sr and ^{100}Zr is very different from that observed for other regions of shape coexistence, for example in ^{74,76}Kr [21] and $^{182−188}$Hg [22] isotopes, where strong mixing makes the change of the ground state properties more gradual.

The local character of the shape change suggests that specific proton and neutron orbitals are responsible for this effect. Unfortunately, the valence space required to describe A∼100 nuclei is currently too large for conventional shell model calculations, although they could correctly describe the properties of the light (N<60) Zr isotopes [23]. However, recent advances with the Monte Carlo Shell Model have made it possible to investigate the origin of the shape transition at N=60 [24] and relate it to the strong proton-neutron interaction between proton $\pi 1g_{9/2}$ and neutron $\nu 1g_{7/2}$ subshells. Promotion of protons from the $\pi 2p_{1/2}$ to the $\pi 1g_{9/2}$ orbital causes the reduction in the spin-orbit coupling for neutron orbitals, reducing the $\nu 2d_{5/2}$ - $\nu 1g_{7/2}$ gap. Increased occupation of the $\nu 1g_{7/2}$ orbital leads in turn to an increase in spin-orbit splitting in the proton sector and reduction of the $\pi 2p_{1/2}$ - $\pi 1g_{9/2}$ gap. This self-reinforcing effect, known as type-II shell evolution [25], is suggested to be responsible for the appearance of deformed states in Zr isotopes. Since these specific particle-hole excitations lead to a significant reorganization of the effective single-particle energies, the mixing of normal states and those with deformation-optimized shell structure is suppressed, consistent with experimental results. The calculations of Togashi et al. [24] predict a dramatic shape change between the ground states of ^{98}Zr and ^{100}Zr, with the 0^+_2 in ^{98}Zr becoming the 0^+_1 state of ^{100}Zr and the ground state of ^{98}Zr becoming the non-yrast 0^+_2 state in ^{100}Zr and beyond.

The current paper presents new experimental results on lifetimes in neutron-rich Zr isotopes, which bring systematic information on evolution of nuclear deformation and collectivity in the vicinity of the N=60 shape transition. The measured transition strengths are compared to the results of Monte Carlo Shell Model and IBM-1 calculations in order to get a better understanding of the shape transition and configuration inversion in the Zr isotopic chain.

II. EXPERIMENT

Lifetimes of low-lying excited states of ^{98,100,102}Zr have been measured through a prompt-fission spectroscopy experiment performed at the Institut Laue-Langevin (ILL) Grenoble,

France. In this experiment, the high-flux cold neutron beam at PF1B [26] was inducing the fission reactions on targets of ^{235}U and ^{241}Pu. The EXILL-FATIMA setup consisted of 8 EXOGAM clovers and 16 LaBr$_3$(Ce) detectors, which were placed at a distance of 14.5 cm and 8.5 cm, respectively, from the target [27]. Each target was sandwiched between Be layers to stop the fission fragments. The LaBr$_3$(Ce) detectors were arranged in a compact configuration to maximize the number of $\gamma-\gamma$ coincidences. A detailed description of the collimation of the neutron beam can be found in Ref. [28], the detector arrangement and analogue fast-timing electronics in Ref. [27] and the trigger-less data acquisition system in Ref. [29].

A. Data analysis

The data were sorted using a C++ based software, SO-COv2 [30], developed in the Institute of Nuclear Physics, Cologne. For the present application, coincidences between exactly one clover (after add-back) and two LaBr$_3$(Ce) detectors were required within the 120 ns time window, meaning the γ-ray multiplicity was equal to three.

The modern fast-timing method of Mirror Symmetric Centroid Difference (MSCD) [31] was used in the present work for lifetime determination. By using the feeding (decay) transition of a sequential $\gamma-\gamma$ cascade as the start signal of a Time-to-Amplitude converter (TAC) module and the decay (feeder) transition as the stop, we observed a signal delayed (anti-delayed) by the lifetime τ of the decaying state. The centroid of the resulting TAC spectrum is thus shifted by τ (respectively -τ) from its prompt position. The MSCD method is based on the difference between the centroids of these two independent time distributions of a sequential $\gamma-\gamma$ cascade. This method considers the centroid difference as a physical observable and as the name suggests, interprets the centroid difference of the $\gamma-\gamma$ cascade as mirror symmetric with respect to a start-stop inversion, or equivalently, to a hypothetical inversion of the transitions in the cascade. The MSCD method in the case of no background is described by the following equation:

$$\begin{aligned}
\triangle C(E_{\text{feeder}}, E_{\text{decay}}) &= C_{\text{delayed}} - C_{\text{anti-delayed}} \\
&= C^D(E_{\text{feeder}}, E_{\text{decay}}) - C^{AD}(E_{\text{decay}}, E_{\text{feeder}}) \\
&= PRD(E_{\text{feeder}}, E_{\text{decay}}) + 2\tau, \quad (1)
\end{aligned}$$

where C^D describes the centroid of the delayed time distribution and C^{AD} is the centroid of the anti-delayed one. The PRD is the Prompt Response Difference which describes the combined $\gamma-\gamma$ time-walk of the setup. The PRD for two γ-ray energies in a $\gamma-\gamma$ cascade is given as:

$$PRD(E_{\text{feeder}}, E_{\text{decay}}) = PRD(E_{\text{feeder}}) - PRD(E_{\text{decay}}) \quad (2)$$

and

$$\begin{aligned}
PRD(E_{\text{feeder}}, E_{\text{decay}}) &= PRD_{E_{\text{decay}}}(E_{\text{feeder}}) \\
&= -PRD_{E_{\text{feeder}}}(E_{\text{decay}}), \quad (3)
\end{aligned}$$

where $PRD_{E_{\text{decay}}}(E_{\text{feeder}})$ (respectively $PRD_{E_{\text{feeder}}}(E_{\text{decay}})$) is the Prompt Response Difference at the energy of the feeding

(resp. decay) transition when the reference energy is at the decay (resp. feeding) transition. This shows the mirror symmetry of the method in which both PRD and centroid difference are mirror symmetric.

The PRD calibration is performed using a standard ^{152}Eu source. The calculated PRD has been fitted by using the following calibration equation:

$$PRD(E_\gamma) = \frac{a}{\sqrt{b + E_\gamma}} + c.E_\gamma + d.E_\gamma^2 + e, \quad (4)$$

where a, b, c, d and e are the fit parameters. In the present case the PRD curve is adjusted for E_{ref} = 344 keV (i.e., the value of the PRD at 344 keV is 0 ps). The uncertainty on the PRD, δ(PRD), was obtained from the fit residual (mean root squared derivation) and is equal to 10 ps within the 3σ limit. The PRD curve (shown in Fig. 2) can be used to read the PRD value for any sequential $\gamma-\gamma$ cascade within the energy range of 0 – 1400 keV. The anode pulse was used for timing since it provides a stable, count-rate independent signal which results in a constant time-walk characteristics, i.e., the shape of the PRD curve does not change. This has been explored and verified from data collected over 5 weeks using different γ-ray sources and (n,γ) reactions with detector count rates ranging from 3 to 25 kHz [27]. The determination of the timing uncertainties and the PRD calibration procedure of the EXILL-FATIMA setup are described in detail in [27].
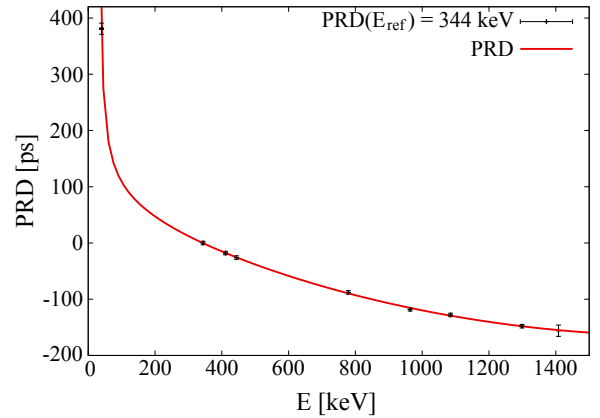

FIG. 2. PRD curve obtained using a ^{152}Eu source.

The MSCD method has been extended to the Generalized Centroid Difference Method (GCDM) for the system of N nearly identical fast-timing detectors, as in the case of the EXILL-FATIMA campaign. In this method, instead of evaluating individual centroid differences for 'C$_{start,stop}$' between two independent timing distributions, the superimposed TAC spectrum of all the combinations of 'start, stop' belonging to the N-detector system is evaluated [32]. Similar to equation 1, the relation between the mean centroid difference $(\overline{\triangle C(E_\gamma)})$ and the mean Prompt Response Difference $(\overline{PRD})$ is given by:

$$\overline{\triangle C_{FEP}} = \overline{PRD} + 2\tau, \quad (5)$$

where FEP stands for full-energy peak. Equation 5 is valid if the time differences between the start and the stop events are statistically distributed around the mean $\overline{\triangle C_{FEP}}$ or $\overline{PRD}$, and are independent of the detector-detector combination.

B. Lifetime determination

We have measured the lifetimes of the 2_1^+ and 4_1^+ states of ^{98}Zr and 2_1^+, 4_1^+ and 6_1^+ states of ^{100,102}Zr, analyzing the data collected with each of the targets (^{235}U and ^{241}Pu) separately. We present the details of the analysis procedure using the examples of the 2_1^+ and 4_1^+ states of ^{100,102}Zr.

The most prominent source of background in the low-energy range (≤ 300 keV) for the EXILL-FATIMA setup was the Compton scattering. It arises from the superposition of Compton continua of multiple γ rays produced in the fission process. In an ideal setup, Eq. 5 can be used for lifetime determination, however, in a real setup the experimental centroid difference ($\triangle C_{exp}$) must be corrected in order to account for the Compton background ($\triangle C_{BG}$), following:

$$\triangle C_{FEP} = \triangle C_{exp} + \frac{\triangle C_{exp} - \triangle C_{BG}}{p/b}, \qquad (6)$$

where p/b is the peak to background ratio. Equation 6 can be used for the Compton background correction when only one background component is present [27, 31]. However, since two FEP's (feeder and decay) are used in the lifetime analysis, the Compton background underneath each of the FEP's in the γ-γ cascade must be considered separately [15]:

$$\triangle C_{FEP} = \triangle C_{exp} + \frac{1}{2}\Big[t_{corr}(\text{feeder}) + t_{corr}(\text{decay})\Big], \qquad (7)$$

where,

$$t_{corr}(\text{feeder}) = \left[\frac{(\triangle C_{exp} - \triangle C_{BG})}{p/b}\right]_{\text{feeder}},$$
$$t_{corr}(\text{decay}) = \left[\frac{(\triangle C_{exp} - \triangle C_{BG})}{p/b}\right]_{\text{decay}}, \qquad (8)$$

and

$$\tau = \frac{1}{2}(\triangle C_{FEP} - PRD) \qquad (9)$$

In Eqs. 7 and 9, $\triangle C_{exp}$ is the experimental value, $\triangle C_{FEP}$ is the one related to FEP events only, corrected for the contribution of the Compton background ($\triangle C_{BG}$). The term t_{corr}(feeder) (resp. t_{corr}(decay)) in Eq. 8 is the background correction resulting from the feeding (decay) transition in a spectrum gated on the decay (feeding) transition, and hence at the reference energy (E_{ref}). When estimating the uncertainty on the lifetime, the individual contributions are taken into account as follows:

$$\delta\tau = \frac{1}{2}\sqrt{\delta\triangle C_{exp}{}^2 + \delta t_{corr}{}^2 + \delta PRD^2}, \qquad (10)$$

where δt_{corr} corresponds to the mean uncertainty of the two Compton background correction terms.

The high multiplicity of γ rays produced in the fission process can sometimes lead to erroneous results. For example, the transitions of interest (feeder and decay) for the lifetime measurements of 4_1^+ and 6_1^+ states of ^{100,102}Zr lie in the same energy range (480-500 keV) as the low-lying γ-ray transitions in ^{138}Xe. ^{138}Xe is one of the possible complementary partners of both ^{100}Zr and ^{102}Zr in the ^{241}Pu fission, through:

$$^{241}_{94}\text{Pu} + n_{th} \longrightarrow {}^{102}_{40}\text{Zr}_{62} + {}^{138}_{54}\text{Xe}, \; 2n \text{ emission}$$
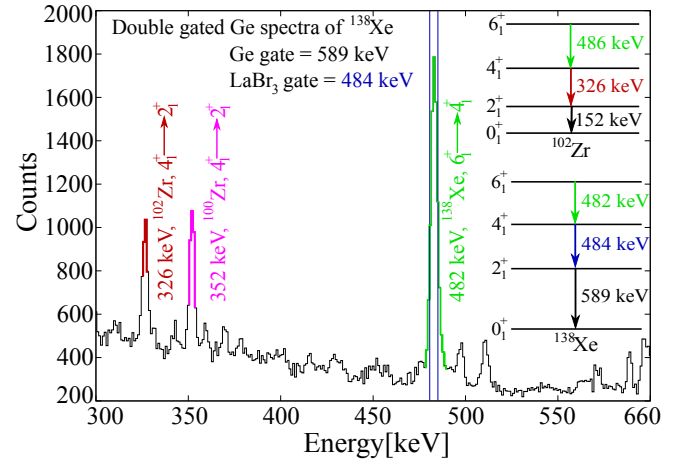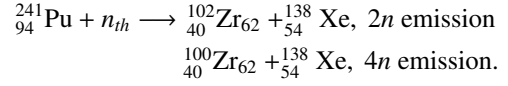$$^{100}_{40}\text{Zr}_{62} + {}^{138}_{54}\text{Xe}, \; 4n \text{ emission}.$$

FIG. 3. The double-gated spectrum of ^{138}Xe which is a complementary partner of ^{100}Zr and ^{102}Zr. Prominent peaks in the spectrum (shown in different colors) correspond to transitions in ^{100}Zr, ^{102}Zr and ^{138}Xe.

This is illustrated by Fig. 3 showing a double-gated (Ge + LaBr$_3$) spectrum of ^{241}Pu fission products, gated on two transitions in ^{138}Xe: $2_1^+ \longrightarrow 0_1^+$ (589 keV) observed with the Ge detectors and $4_1^+ \longrightarrow 2_1^+$ (484 keV) with LaBr$_3$(Ce) detectors. In addition to prominent γ rays in ^{138}Xe, one can also see γ rays (highlighted in Fig. 3) originating from ^{100,102}Zr, proving that ^{138}Xe and ^{100,102}Zr are complementary partners. As these nuclei happen to have transitions with almost identical energies, the time spectra gated on the 486 keV from ^{102}Zr and 497 keV from ^{100}Zr will be contaminated by the 482 keV and 484 keV from ^{138}Xe, resulting in biased lifetimes. This is, however, not the case for the fission of ^{235}U, where Te nuclei are fission partners of ^{100,102}Zr, and thus the lifetimes of 4_1^+ and 6_1^+ state of ^{100,102}Zr can be correctly determined from the latter data set.

1. ^{98}Zr

Level lifetimes in ^{98}Zr were investigated for the 2_1^+ and 4_1^+ states. The lifetime analysis for the 2_1^+ state is done by using the 1223 keV $2_1^+ \longrightarrow 0_1^+$ transition depopulating this state

as a stop and that feeding it (621 keV, $4_1^+ \longrightarrow 2_1^+$) as a start. The latter is used as the reference for the PRD. In addition, a gate on Ge singles is applied on the $6_1^+ \longrightarrow 4_1^+$ transition at 647 keV to select the cascade of interest and to improve the peak-to-background ratio. The correction for Compton background that lies underneath the peak of interest is applied using Eq. 7. Due to the uncertainties in PRD and Compton background correction for both fission targets, the lifetime of the short-lived 2_1^+ level of ^{98}Zr could not be determined precisely and only an upper limit is obtained. The feeding (647 keV) and the decay (621 keV) transition of the 4_1^+ level of ^{98}Zr are very close in energy and the energy resolution of the LaBr$_3$ detectors for EXILL-FATIMA array is not sufficient to distinguish unambiguously between these energies. Therefore, the summed lifetime of the 2_1^+ and 4_1^+ state of ^{98}Zr is measured and without a precise lifetime on the 2_1^+ state only an upper limit is obtained on the lifetime of the 4_1^+ state.

2. ^{100}Zr

The lifetimes of the 2_1^+ and 4_1^+ states of ^{100}Zr were determined using GCDM as explained in Sec. II A. In addition, the slope method was also used to extract the 2_1^+ lifetime, as shown in Fig. 4. The spectra in Fig. 4(b), in contrast to those in Fig. 4(a), display two slope components, a fast (small bump at the beginning) and a slow one. Especially for lifetimes below 1 ns, it is difficult to distinguish between the two slope components and select the time range in which only the slow slope component will be fitted. The different precision on the lifetime obtained using data from each of the fission targets is due to a better peak-to-background ratio in the ^{235}U data. For comparison, if we try to apply Eq. 9 to $\triangle C_{exp}$ values from Fig. 4 in order to extract the lifetime assuming no background, we obtain significantly different values (603(11) ps for ^{235}U target and 509(9) ps for ^{241}Pu) from those extracted using the slope method. This demonstrates that for lifetimes below 1 ns the correction for Compton background should be performed, and consequently we further apply the GCDM with its reliable background correction procedure to the 2_1^+ state of ^{100}Zr.

Fig. 5 illustrates the complete GCDM procedure for the lifetime evaluation of the 2_1^+ state of ^{100}Zr with ^{241}Pu as a fission target. Fig. 5(a) presents the double-gated (Ge + LaBr$_3$) spectrum with E$_{ref}$ of 352 keV (transition feeding the 2_1^+ state) and FEP is the decay of the 2_1^+ state at E=212 keV. A narrow energy gate of 6 keV is applied on the FEP and the two centroids of independent delayed and anti-delayed time distributions are calculated. The difference between these two time distribution centroids yields the $\triangle C_{exp}$ value. The Compton background correction is performed by: 1) finding the time distribution of the background through gating on a few background points in the vicinity of the FEP using the same channel width (6 channels), 2) plotting the centroid difference of these background points against their respective energy, 3) fitting this dependence using a polynomial function, and 4) reading the $\triangle C_{BG}$ at the position of the FEP from the thus obtained background curve (as shown in Fig. 5(c)). The PRD correction is directly read from the PRD curve in Fig. 5(c). This
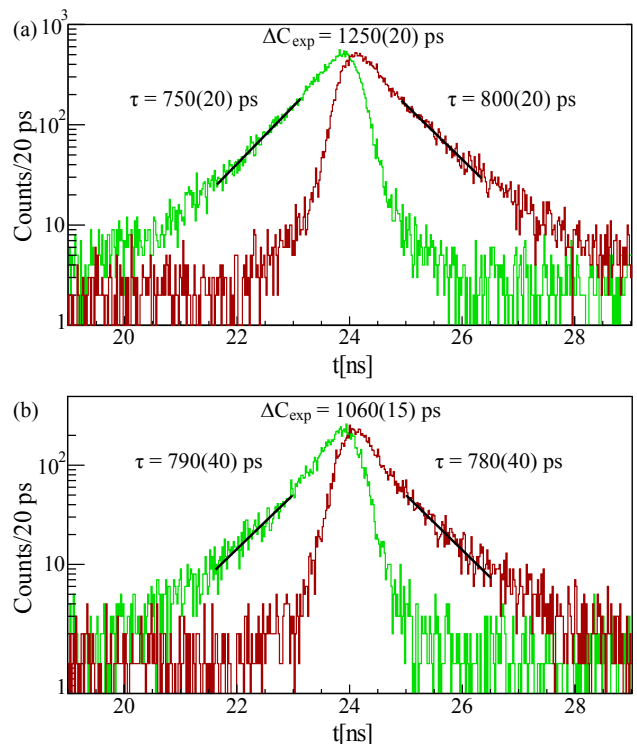

FIG. 4. Lifetime determination using the slope method for the 2_1^+ state of ^{100}Zr. (a) displays the delayed (red) and the anti-delayed (green/light gray) time distributions of the state of interest from ^{235}U fission, and (b) from ^{241}Pu fission.

curve is shifted with respect to the original plot (Fig. 2, details in Ref. [27]) in order to yield PRD equal to 0 at E$_{ref}$ of 212 keV.

The same procedure is repeated with the feeding and depopulating transitions interchanged (E$_{ref}$ at 352 keV and FEP at 212 keV). In this case, the background region is different and consequently different background gates are applied. It should be noted that the PRD curve as well as the Compton background correction curve in Fig. 5(d) are inverted with respect to those in Fig. 5(c) since the E$_{ref}$ is flipped from the transition feeding the state of interest to that depopulating it. Equations 7 and 9 are then applied to the values listed in Figs. 5(c) and 5(d) yielding the lifetime of the 2_1^+ level equal to 830(30) ps.

3. ^{102}Zr

The lifetime of the 2_1^+ state of ^{102}Zr was determined using the slope method on data obtained from both targets. Fig. 6 shows the time distribution observed with the ^{241}Pu target. The slow component of the slope is more prominent compared to that observed for ^{100}Zr (Fig. 4) because of the longer lifetime of the 2_1^+ level of ^{102}Zr and a relatively low background contribution to the peak. Consistent values were obtained for both targets: 2.91(15) ns for ^{241}Pu and 2.9(2) ns for ^{235}U.

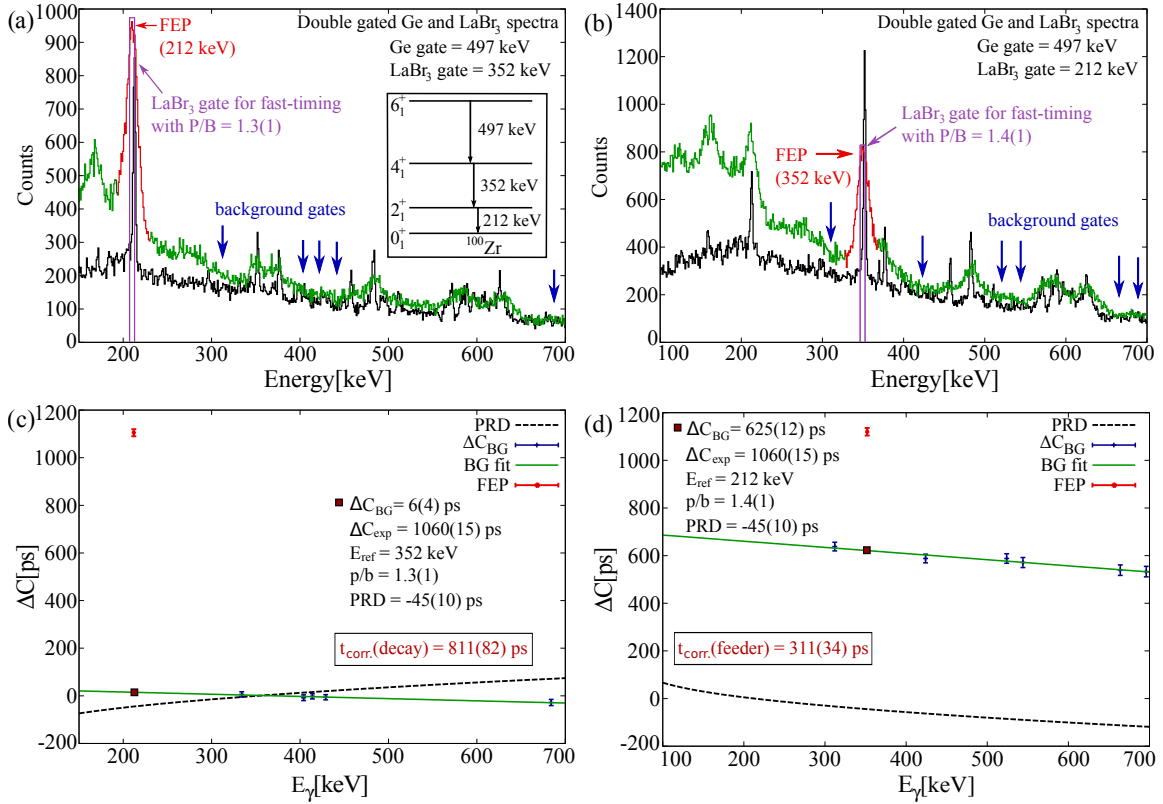To determine the previously unknown lifetimes of the 4_1^+

FIG. 5. Lifetime analysis for the 2_1^+ state in ^{100}Zr. Panels a) and b) show the double-gated Ge (shown in black) and LaBr$_3$ (green/gray) spectra. Panels c) and d) display the Compton background correction procedure (see text for details).

and 6_1^+ states, the GDCM was applied to the data collected using both ^{235}U and ^{241}Pu targets. The lifetime analysis for the 4_1^+ state of ^{102}Zr using the ^{235}U target data is presented in Figs. 7 and 8. It follows the same procedure as for ^{100}Zr except that in this case the centroid difference related to the Compton background ($\triangle C_{BG}$) is fitted using a quadratic function. It is worth mentioning that for this level the background contribution was larger with respect to the FEP as was the $\triangle C_{BG}$ correction. The parallel adjustment of the PRD curve is made as per Eq. 2 in order to cross the energy axis at the reference energy. It should be noted that the PRD curve in Figs. 7(c) and 5(c) does not change its shape for different reference energies and only a parallel shift is observed, which is related to the $\gamma - \gamma$ time walk of the corresponding energies. The lifetimes obtained for the 4_1^+ and 6_1^+ states with the ^{241}Pu target are influenced by the presence in the γ-ray spectra of the transitions in the complementary fission partner ^{138}Xe, as explained in Sec. II B. This is, however, not the case for data collected with the ^{235}U fission target. A value of 46(7) ps was determined for the lifetime of the 4_1^+ state, using t_{corr}(feeder) = 16(5) ps and t_{corr}(decay) = −9(10) ps. For the 6_1^+ state, an upper limit of 12 ps was obtained.
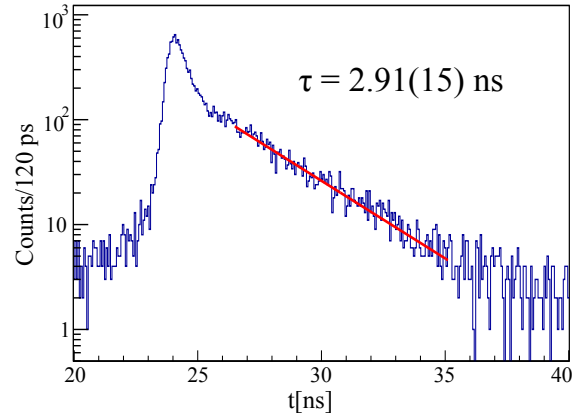

FIG. 6. Lifetime determination for the 2_1^+ state of ^{102}Zr using the ^{241}Pu target data. The independent anti-delayed time spectrum resulting from the FEP events is inverted and aligned before being summed to the delayed time distribution. The slope has been determined by fitting the data in the range from 25.5 ns to 35 ns.
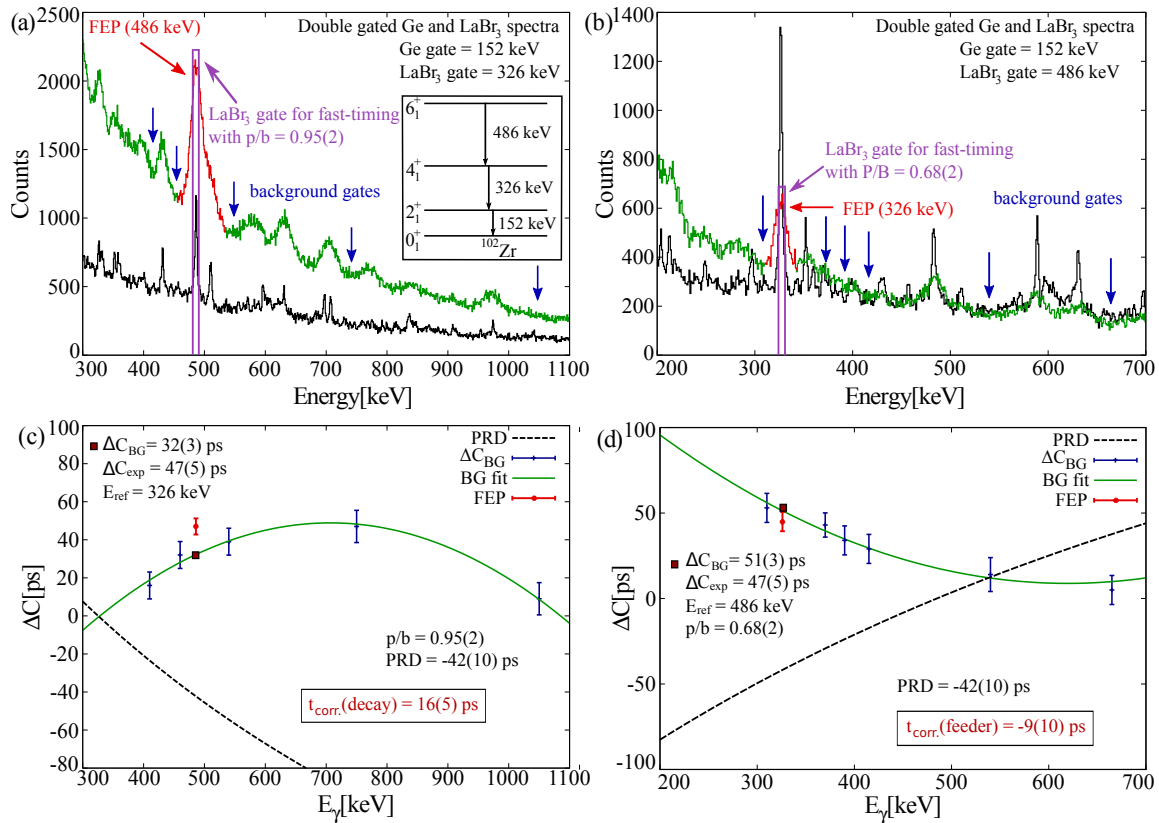
FIG. 7. Lifetime analysis for the 4^+_1 state in ^{102}Zr. Panels a) and b) display double-gated Ge (shown in black) and LaBr$_3$ (green/light gray) spectra. Panels c) and d) show the Compton background correction procedure (see text for details).

III. RESULTS AND DISCUSSION

The obtained lifetimes are presented in Tab. I. Only upper limits could be determined for the 2^+_1 and 4^+_1 states of ^{98}Zr, and the 6^+_1 state of ^{102}Zr, due to the low peak-to-background ratios and short lifetimes. We concluded from the analysis performed for the 2^+_1 state of ^{100}Zr that the slope method is sensitive to background for lifetimes below 1 ns whereas the GCDM gives consistent results for both targets even though the peak-to-background ratio was dramatically different. The lifetimes of the 4^+_1 and 6^+_1 states of ^{100,102}Zr measured using the ^{241}Pu fission target are significantly different from those obtained with ^{235}U. This is related to the contamination of relevant γ-ray spectra by transitions in the complementary fission partner, as explained in Sec. II B.

Lifetimes in ^{98}Zr were previously measured in a $\beta - \gamma - \gamma$ experiment using the centroid shift method [33]. In ^{100}Zr, lifetimes of the short-lived 4^+_1 and 6^+_1 states were measured using Doppler profile method [34, 35] and the long-lived 2^+_1 using different techniques illustrated in [2, 35–40]. Most of these values are in good agreement with the present results as shown in Tab. I.

The present experimental lifetime results are used to calculate the B(E2)↓ transition strengths that are compared with theoretical calculations using the Interacting Boson Model

(IBM-1) [42] and the Monte Carlo Shell Model (MCSM) [24], as shown in Fig. 9.

The IBM-1 calculations, described in detail in Ref. [42], used ^{90}Zr as the core. Good agreement with the present experimental results is found for ^{100,102}Zr. Since only upper limits are currently known for the lifetimes in ^{98}Zr, it is difficult to make firm conclusions on the evolution of transition probabilities from ^{98}Zr to ^{100}Zr, which is predicted by the IBM-1 to be gradual. It should be noted that these calculations also predict a smooth change in the energy of the 2^+_1 state with increasing neutron number, contrary to the experimental observations (see Fig. 1). In contrast, the dramatic decrease of the 2^+_1 level energy when going from ^{98}Zr to ^{100}Zr has been well reproduced by recent state-of-the-art MCSM calculation [24]. Unlike the conventional shell model calculations that are constrained by the size of the configuration space, the MCSM allows the calculation in large configuration spaces up to 3.7 $\times 10^{23}$ two-body matrix elements. Our data on ^{100,102}Zr agree very well with the MCSM predictions, while the obtained upper limit on the 2^+_1 lifetime in ^{98}Zr does not permit the discrimination between the drastic phase transition at N=60 predicted by MCSM and a smooth onset of collectivity as per the IBM-1. Our lower limit on the B(E2 ↓; $4^+_1 \rightarrow 2^+_1$) value in ^{98}Zr is not in agreement with the literature value, but is consistent with both the MCSM and IBM-1 calculations. The upper limit on the lifetime of the 6^+_1 state in ^{102}Zr does not allow for

TABLE I. Lifetimes of yrast states in ^{98,100,102}Zr extracted using fast-timing methods from the ^{241}Pu and ^{235}U data from the EXILL-FATIMA campaign. All values are given in ps unless mentioned otherwise. The literature values are the most recent values from Evaluated and Unevaluated National Nuclear Data Center [7] with the original reference provided. All the lifetime results are quoted with 1σ confidence limit.

Nucleus	J^π	Lifetime (τ) ^{241}Pu	^{235}U	**Adopted**	Literature	B(E2 ↓; $J_1 \to$ J-2$_1$)[W.u.] (adopted)[a]
^{98}Zr	2_1^+	≤ 10	≤ 6	**≤6**	≤ 15 [33]	**≥1.83**
	4_1^+	≤ 20	≤ 15	**≤15**	29(8) [33]	**≥20.75**
^{100}Zr	2_1^+	830(30)	850(20)	**840(18)**	851(43) [2, 35–40]	**76.11$^{+1.75}_{-1.67}$**
	4_1^+	25(10)[b]	37(4)	**37(4)**	53.4(5) [35]	**147.02$^{+17.85}_{-14.36}$**
	6_1^+		12(5)	**12(5)**	7.0(16) [35]	**81.34$^{+58.11}_{-23.92}$**
^{102}Zr	2_1^+	2.91(15) ns	2.91(7) ns	**2.91(8) ns**	2.6(5) ns [41]	**99.46$^{+3.41}_{-3.22}$**
	4_1^+	21(15) [b]	46(7)	**46(7)**	-	**166.95$^{+30.01}_{-22.08}$**
	6_1^+	13(11) [b]	≤ 12	**≤ 12**	-	**≥88**

[a] 1 W.u equals to 26.84, 27.57, 28.31 e^{2}fm^4 in ^{98,100,102}Zr respectively.

[b] The lifetimes determined from the ^{241}Pu data are affected by the contamination from γ-ray transitions in the complementary fission partner as explained in Sec. II B .
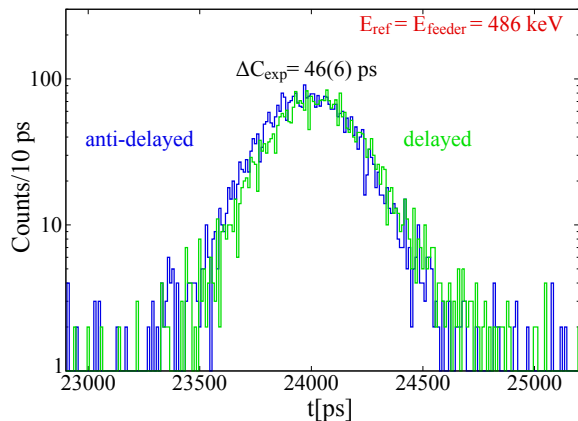

FIG. 8. Two independent time distributions (delayed and anti-delayed) for the 4_1^+ state of ^{102}Zr.

The lifetime of the 4_1^+ state and an upper limit on the lifetime of the 6_1^+ state in ^{102}Zr were obtained for the first time. For other lifetimes determined in this study, good agreement was found with the literature values except for the limit on the 4_1^+ level of ^{98}Zr and the lifetime of the 4_1^+ level of ^{100}Zr. The presently determined upper limits on the lifetimes in the ground-state band of ^{98}Zr do not permit conclusions on the possible shape phase transition in the Zr isotopic chain at N=60.
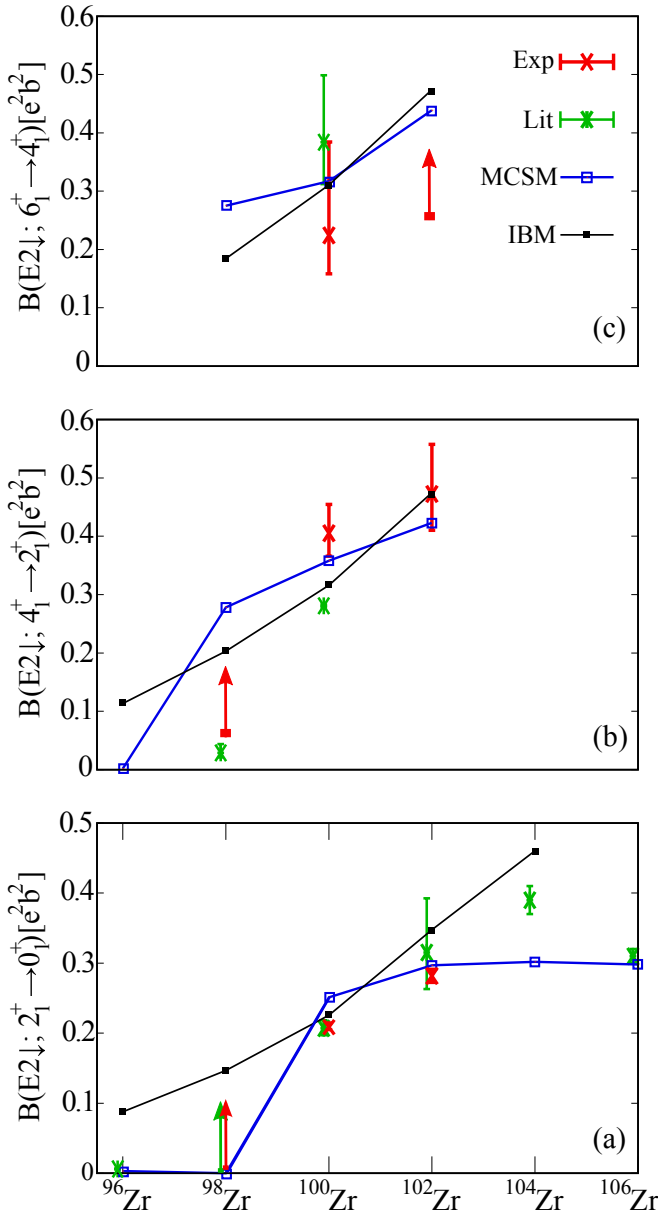
a meaningful comparison with either model predictions. Definite lifetimes in ^{98}Zr are required that will provide the final verdict on the phase transition in this region and also allow us to further investigate the phenomenon of shape coexistence.

IV. SUMMARY

We studied lifetimes of yrast states in ^{98,100,102}Zr populated in neutron-induced fission of ^{241}Pu and ^{235}U using a combination of fast-timing LaBr$_3$(Ce) and EXOGAM clover detectors. The lifetimes were determined using the slope method, applicable for the lifetimes above approximately 1 ns, and the Generalized Centroid Difference Method for shorter lifetimes.

FIG. 9. Known B(E2 ↓; $2_1^+ \rightarrow 0_1^+$), B(E2 ↓; $4_1^+ \rightarrow 2_1^+$) and B(E2 ↓; $6_1^+ \rightarrow 4_1^+$) values (panel a, b and c, respectively) in ^{98,100,102,104,106}Zr, compared with the IBM-1 [42] and MCSM [24] calculations. The B(E2)↓ values obtained in the present study (see Table I) are plotted in red and and the literature values [2, 33–41, 43, 44] in green/light gray. All values are expressed in e^2b^2.

ACKNOWLEDGEMENTS

[1] S. A. Johansson, Nuclear Physics **64**, 147 (1965).

[2] E. Cheifetz, R. C. Jared, S. G. Thompson, and J. B. Wilhelmy, Phys. Rev. Lett. **25**, 38 (1970).

[3] D. Arseniev, A. Sobiczewski, and V. Soloviev, Nuclear Physics A **139**, 269 (1969).

[4] R. Sheline, I. Ragnarsson, and S. Nilsson, Physics Letters B **41**, 115 (1972).

[5] S. Naimi, G. Audi, D. Beck, K. Blaum, C. Böhm, *et al.*, Phys. Rev. Lett. **105**, 032502 (2010).

[6] F. Flavigny, P. Doornenbal, A. Obertelli, J.-P. Delaroche, M. Girod, *et al.*, Phys. Rev. Lett. **118**, 242501 (2017).

[7] M. Chadwick, M. Herman, P. Obložinský, *et al.*, Nuclear Data Sheets **112**, 2887 (2011), special Issue on ENDF/B-VII.1 Library.

[8] J. Dudouet, A. Lemasson, G. Duchêne, M. Rejmund, E. Clément, C. Michelagnoli, F. Didierjean, *et al.*, Phys. Rev. Lett. **118**, 162501 (2017).

[9] M. Albers, N. Warr, K. Nomura, A. Blazhev, J. Jolie, *et al.*, Phys. Rev. Lett. **108**, 062701 (2012), errata: **109**, 209904 and **114**, 189902.

[10] C. Sotty, M. Zielińska, G. Georgiev, D. L. Balabanski, A. E. Stuchbery, A. Blazhev, *et al.*, Phys. Rev. Lett. **115**, 172501 (2015).

[11] T. W. Hagen, A. Görgen, W. Korten, L. Grente, M.-D. Salsac, *et al.*, Phys. Rev. C **95**, 034302 (2017).

[12] K. Heyde and J. L. Wood, Rev. Mod. Phys. **83**, 1467 (2011).

[13] E. Clément, M. Zielińska, A. Görgen, W. Korten, S. Péru, *et al.*, Phys. Rev. Lett. **116**, 022701 (2016).

[14] E. Clément, M. Zielińska, *et al.*, Phys. Rev. C **94**, 054326 (2016).

[15] J.-M. Régis, J. Jolie, N. Saed-Samii, N. Warr, *et al.*, Phys. Rev. C **95**, 054319 (2017), erratum: **95**, 069902.

[16] F. Schussler, J. Pinston, E. Monnand, A. Moussa, G. Jung, and other, Nuclear Physics A **339**, 415 (1980).

[17] J. Park, A. B. Garnsworthy, R. Krücken, C. Andreoiu, G. C. Ball, P. C. Bender, A. Chester, A. Close, P. Finlay, P. E. Garrett, *et al.*, Phys. Rev. C **93**, 014315 (2016).

[18] F. Wohn, H. Mach, M. Moszyǹski, R. Gill, and R. Casten, Nuclear Physics A **507**, 141 (1990).

[19] H. Mach, M. Moszyǹski, R. L. Gill, G. Molnár, F. K. Wohn, J. A. Winger, and J. C. Hill, Phys. Rev. C **41**, 350 (1990).

[20] C. Y. Wu, H. Hua, and D. Cline, Phys. Rev. C **68**, 034322 (2003).

[21] E. Clément, A. Görgen, W. Korten, E. Bouchez, A. Chatillon, J.-P. Delaroche, *et al.*, Phys. Rev. C **75**, 054313 (2007).

[22] N. Bree, K. Wrzosek-Lipska, A. Petts, A. Andreyev, B. Bastin, *et al.*, Phys. Rev. Lett. **112**, 162701 (2014).

[23] K. Sieja, F. Nowacki, K. Langanke, and G. Martínez-Pinedo, Phys. Rev. C **79**, 064310 (2009).

[24] T. Togashi, Y. Tsunoda, T. Otsuka, and N. Shimizu, Phys. Rev. Lett. **117**, 172502 (2016).

[25] T. Otsuka and Y. Tsunoda, Journal of Physics G: Nuclear and Particle Physics **43**, 024009 (2016).

[26] H. Abele, D. Dubbers, H. Häse, M. Klein, A. Knöpfler, M. Kreuz, T. Lauer, B. Märkisch, *et al.*, Nuclear Instruments and Methods in Physics Research Section A **562**, 407 (2006).

[27] J.-M. Régis, G. Simpson, A. Blanc, G. de France, M. Jentschel, U. Köster, P. Mutti, *et al.*, Nuclear Instruments and Methods in Physics Research Section A **763**, 210 (2014).

[28] W. Urban, M. Jentschel, B. Mrkisch, T. Materna, C. Bernards, C. Drescher, C. Fransen, J. Jolie, U. Köster, P. Mutti, T. Rzaca-Urban, and G. S. Simpson, Journal of Instrumentation **8**, P03014 (2013).

[29] P. Mutti, A. Blanc, G. de France, M. Jentschel, U. Köster, E. R. Martinez, G. Simpson, T. Soldner, C. A. Ur, and W. Urban, Advancements in Nuclear Instrumentation Measurement Methods and their Applications (ANIMMA) , 1 (2013).

[30] N. Saed-Samii, Diploma thesis (unpublished), Institute of Nuclear Physics, Cologne (2015).

[31] J.-M. Régis, G. Pascovici, J. Jolie, and M. Rudigier, Nuclear Instruments and Methods in Physics Research Section A **622**, 83 (2010).

[32] J.-M. Régis, H. Mach, G. Simpson, J. Jolie, G. Pascovici, N. Saed-Samii, N. Warr, *et al.*, Nuclear Instruments and Methods in Physics Research Section A **726**, 191 (2013).

[33] L. Bettermann, J.-M. Régis, T. Materna, J. Jolie, U. Köster, K. Moschner, and D. Radeck, Phys. Rev. C **82**, 044310 (2010).

[34] A. Smith, D. Patel, G. Simpson, R. Wall, J. Smith, O. Onakanmi, I. Ahmad, J. Greene, *et al.*, Physics Letters B **591**, 55 (2004).

[35] A. G. Smith, R. M. Wall, D. Patel, G. S. Simpson, D. M. Cullen, J. L. Durell, S. J. Freeman, *et al.*, Journal of Physics G: Nuclear and Particle Physics **28**, 2307 (2002).

[36] H. Mach, M. Moszynǹski, R. Gill, F. Wohn, J. Winger, J. C. Hill, G. Molnár, and K. Sistemich, Physics Letters B **230**, 21 (1989).

[37] H. Ohm, M. Liang, G. Molnar, and K. Sistemich, Z.Phys. **A334**, 519 (1989).

[38] G. Lhersonneau, H. Gabelmann, N. Kaffrell, K. L. Kratz, B. Pfeiffer, and the ISOLDE Collaboration, Z.Phys. **A332**, 243 (1989).

[39] E. Cheifetz, H. A. Selic, A. Wolf, R. Chechik, and J. B. Wilhelmy, in *Proc.Conf.Nucl.Spectr.Fission Products* (1980).

[40] R. C. Jared, H. Nifenecker, and S. G. Thompson, in *Proc.Symp.Phys.Chem.Fission* (1974).

[41] S. Raman, C. Nestor, and P. Tikkanen, Atomic Data and Nuclear Data Tables **78**, 1 (2001).

[42] J. E. García-Ramos, K. Heyde, R. Fossion, V. Hellemans, and S. De Baerdemacker, The European Physical Journal A - Hadrons and Nuclei **26**, 221 (2005).

[43] F. Browne, A. Bruce, T. Sumikama, I. Nishizuka, S. Nishimura, P. Doornenbal, *et al.*, Physics Letters B **750**, 448 (2015).

[44] G. Kumbartzki, N. Benczer-Koller, J. Holden, G. Jakob, T. Mertzimekis, *et al.*, Physics Letters B **562**, 193 (2003).